

# A 5-WATT, 37-GHz MONOLITHIC GRID AMPLIFIER

Blythe Deckman<sup>1</sup>, Donald S. Deakin, Jr.<sup>2</sup>, Emilio Sovero<sup>2</sup>, David Rutledge<sup>1</sup>

<sup>1</sup>Department of Electrical Engineering, California Institute of Technology, Pasadena, CA 91125

<sup>2</sup>Rockwell Science Center, Thousand Oaks, CA 91358

**Abstract**—A 5-Watt Ka-band amplifier has been demonstrated. The area of the grid amplifier is  $1\text{ cm}^2$ , and there are 512 transistors. The small-signal gain of the grid is 8 dB at 37.2 GHz, with 1.3 GHz bandwidth. At 5 Watts output, the gain is 5 dB with 15% power-added efficiency. An aluminum-nitride heat spreader allows continuous operation with an estimated gate temperature of  $70^\circ\text{C}$ .

## Introduction

The use of spatial power combiners as an efficient method to incorporate the outputs of many solid state amplifiers has in recent years drawn significant research effort. Liu *et al.* demonstrated a 44-GHz monolithic grid amplifier that gave 670 mW with a power-added efficiency of 4% [1]. Hacker *et al.* recently demonstrated a monolithic  $1.44\text{ cm}^2$  amplifier that gave 1.8 W with 3.7-dB gain at 38.6 GHz [2]. Hybrid amplifiers have also been successfully demonstrated with higher powers [3, 4]. Recent advances in computer speed and field simulators have facilitated the development of accurate modeling techniques [5].

Here we demonstrate a monolithic grid amplifier that shows 8-dB small-signal gain, 1.3-GHz bandwidth, and delivers 5 W of power at 37.2 GHz with 5-dB gain. Devices used here are  $80\text{-}\mu\text{m}$  by  $0.18\text{-}\mu\text{m}$  GaAs *p*HEMTs, capable of delivering 11 mW of power at 39 GHz in load pull measurements. The grid uses 512 such *p*HEMTs, giving a total gate width of 41 mm. Figure 1 shows the basic grid amplifier layout and simplified detail of the unit cell. The unit cell uses two transistors connected as a differential pair. Modeling of the amplifier is after [5], exploiting the symmetry of the grid to analyze the structure as a single unit cell. Figure 2 shows a photograph of a corner of the fabricated active grid.

## Thermal Management

Previous grid amplifiers lacked a heat spreader, so

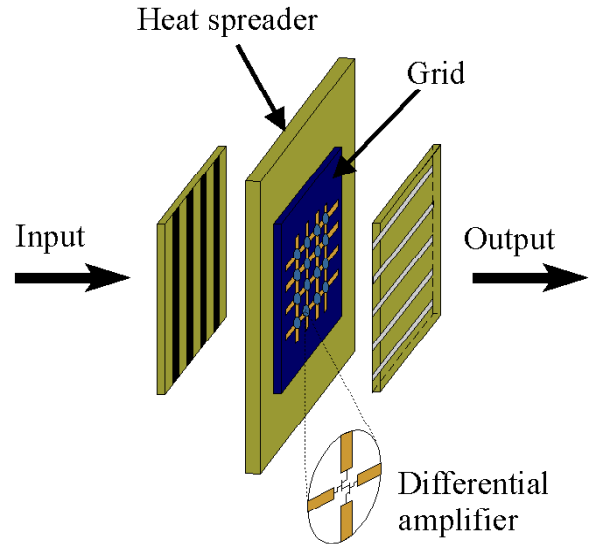


**Figure 1.** Basic grid layout and simplified unit cell layout. Two devices operate in differential mode. The input beam enters from the left, and changes polarization as it is amplified. The output radiates to the right.

they could only be biased for short periods of time. The grid amplifier in [1] gave 670 mW, with 4% power-added efficiency, leaving 16 W of waste heat to be dissipated. The active devices were fabricated on a GaAs substrate  $635\text{ }\mu\text{m}$  thick, and the GaAs was mounted on a Duroid carrier. Both GaAs and duroid are quite poor thermal conductors, so the grid could be biased for only 0.6 seconds and required a 3-minute cooling time.

In the current work, the devices were fabricated on a GaAs substrate thinned to  $75\text{ }\mu\text{m}$  and mounted on an aluminum-nitride heat spreader 2 mm thick (thermal constant  $170\text{ W/cm}^2$ ). The carrier was then mounted into a Lucite frame, and water circulated around the edges to dissipate the heat.

Using a finite-element heat simulator by Tanner Research, the thermal resistance of the bulk of the GaAs substrate was predicted at approximately  $1^\circ\text{C/W}$ . Heat simulations were also performed for individual amplification cells giving a predicted temperature of the device

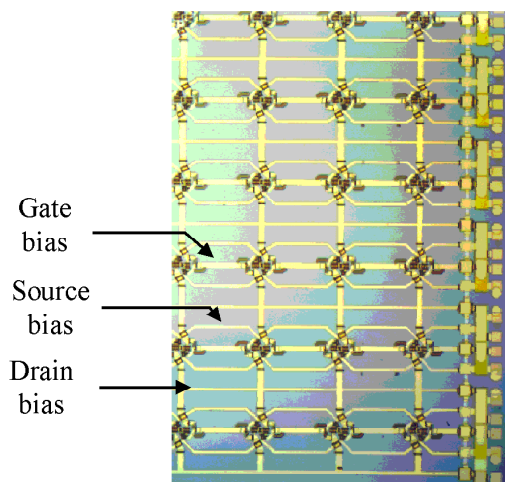


**Figure 2.** Photograph of the grid amplifier. The period of the grid is  $625\ \mu\text{m}$ .

junctions at  $13^\circ\text{C}$  above the substrate. Measurements of a fully biased grid (using a mercury thermometer) operating with the cooler running showed a bulk thermal resistance of  $0.8^\circ\text{C}/\text{W}$ .

Thermal measurements of a fully biased grid were also made using a Thermacam PM290 infrared camera. Since GaAs is transparent to the infrared wavelengths detected by the camera, the thermal image mainly showed the heat profile of the thermal polymer used to attach the GaAs substrate to the heat spreader. The thermal emissivity of the system was calibrated by placing a piece of black electrical tape (with known emissivity of 0.95) next to the grid on the carrier, and measuring the temperature of the tape. The camera was then focused on an area of the grid amplifier free from lens reflections, and the measurement emissivity adjusted until the measurement temperature matched the recorded temperature of the black tape. Thermal measurements of the grid amplifier gave peak temperatures of  $60^\circ\text{C}$ , a result consistent with the simulated peak temperature of  $55^\circ\text{C}$ . The resolution of the lens used for the thermal measurement is  $100\ \mu\text{m}$ , so the individual device gates are not resolvable.

### Bias Lines

Optimal power performance of the grid's transistors requires a gate-source voltage of about  $-0.3\ \text{V}$ . Drops in the source bias lines, then, cause significantly different gate-source bias voltages for devices near the center of the grid. Consequently, two straight gold traces were chosen to carry the bias current, and the bias supplies were connected to both ends of the grid amplifier-chip.

Source bias lines were fabricated  $3\ \mu\text{m}$  thick and  $25\ \mu\text{m}$  wide. The shunt reactance introduced by the bias lines is tuned out by appropriately positioning the polarizers.

Since the gates of the transistors draw negligible DC current, the gate voltage is supplied to the transistors via the same gate trace that is used to detect the incident beam. The gate voltage is passed from one device in a cell to the other through a  $2\text{-k}\Omega$  resistor, providing RF isolation from the virtual ground in the center of the unit cell.

### Stability

Figure 3 shows that the uncompensated devices used in this work are potentially unstable across most of the band of interest. A typical amplifier design (using microstrip, for example) that uses a potentially unstable device usually proceeds by selecting source and load reflection coefficients that avoid the unstable operating conditions of the device. The stability of the constructed amplifier, then, depends on the precision with which the source and load reflection coefficients can be controlled. Grid amplifiers, however, require dynamic tuning of the input and output by adjusting the positions of the polarizers. Such tuning adjustments can cause the source and load reflection coefficients to vary widely, easily falling into unstable regions. To protect the amplifier from oscillations while tuning, resistive feedback of  $1,245\ \Omega$  is used to stabilize the devices over the entire band of interest. A DC blocking capacitor is used to protect the gate bias. Figure 3 also shows the

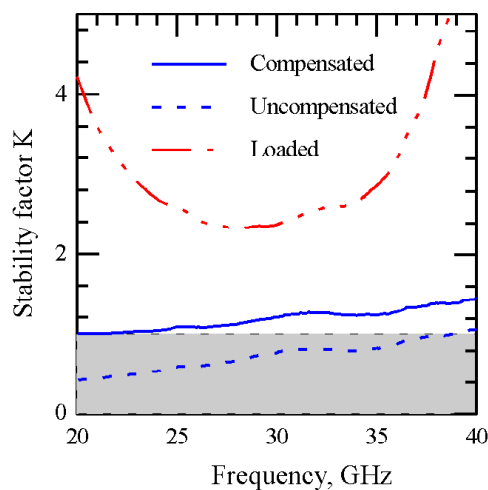


**Figure 3.** Uncompensated, compensated, and loaded stability factors. The grid stability factor includes free-space loading of the input and output sides of the grid amplifier.

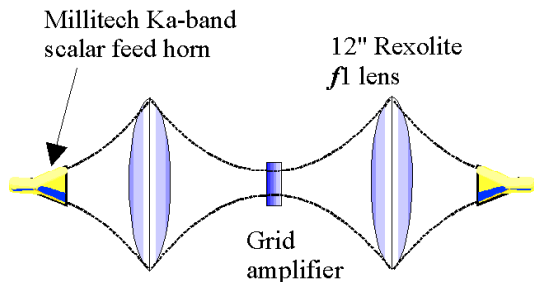


**Figure 4.** Gaussian beam measurement setup. Lenses are two plano-convex lenses held back-to-back. An HP8722D network analyzer drives the horns, and a TWT is added for power measurements.

stability factor of the feedback-compensated device. As shown in the figure, the device is stable at all frequencies between 20 and 40 GHz.

### Measurements

Figure 4 shows a schematic view of the measurement setup used here, and it is after [5]. An HP8722 network analyzer feeds a Millitech scalar horn that launches a gaussian diverging beam toward the input convex lens. The input lens focuses the beam to a spot at the measurement plane where the grid amplifier is placed. The output from the grid is focused by the output lens into another Millitech scalar horn, and then detected by the network analyzer.

Calibration of the system is performed by inserting a polarizer (of equal area to the grid amplifier) into the measurement plane, and rotating it  $45^\circ$  with respect to the polarization of the incident beam. The receive horn is then rotated  $90^\circ$  with respect to the input horn polarization. The polarizer in the measurement plane intercepts the same power as the grid amplifier, but reflects half of it back to the input horn. What the polarizer transmits is polarized at  $45^\circ$  respect to both transmit and receive horns. An orthomode transducer at the back of the receive horn splits the  $45^\circ$  polarized beam equally between its two ports, and the network analyzer is connected to one of them (the second is terminated). As such, 25% of the power incident on the polarizer is detected by the network analyzer, which is used to calculate the calibration factor.

Small-signal performance of the grid amplifier was measured by placing the grid in the measurement plane after calibration; figure 5 shows the data. The peak gain of the grid is 8 dB with a 3-dB bandwidth of 1.3 GHz. The time-gating functions of the network analyzer were used to eliminate spurious reflections.

Calibration of the network analyzer for power mea-

surements proceeds exactly as for small-signal measurements, but a traveling-wave tube (TWT), built by Amplifier Research, is inserted before the transmit horn, so that its gain is calibrated out. Also, a 30-dB coupler is inserted to sense the incident power from the TWT. With the TWT present in the system, incident powers of greater than 5 W can be achieved.

Following calibration, power measurement proceeds by increasing the network analyzer test port power until the gain of the grid amplifier is saturated. The incident power is calculated from the calibration factor applied to the input power-meter reading. Output power is then calculated by adding the gain of the grid to the incident power. Figure 6 shows the power and gain of the amplifier. As shown, the grid amplifier delivers 5 W with 5-dB gain. Figure 7 shows the drain and power-added efficiencies of the grid.

Under maximum output power conditions, two spurious oscillations were observed at 46 GHz, and at 47 GHz. The strength of both spurs was measured to be 55 dB below the carrier. The spurs are most likely caused by changes in transistor scattering parameters between design and fabrication. Liu's analysis [6], using measured scattering parameters from the fabricated wafer, predicts the spurs.

A comparison between isolated transistor power performance and grid power performance is shown in Fig-

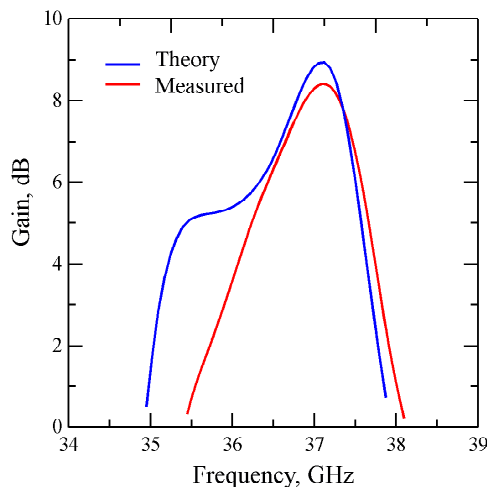


**Figure 5.** Theory and experiment for small-signal gain. In the measurement, the polarizer on the input side is  $500\ \mu\text{m}$  closer than in the model. This polarizer is suspended inside the cooling frame by a wire arm, and hence cannot be visually set. For this reason, there may be errors in position or angle.

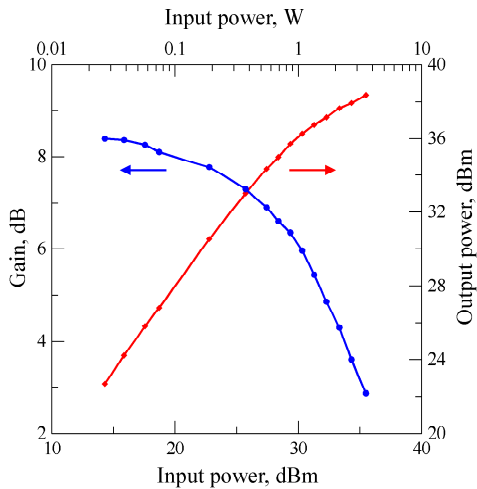


**Figure 6.** Power and gain. The gain at 5 W output is 5 dB.

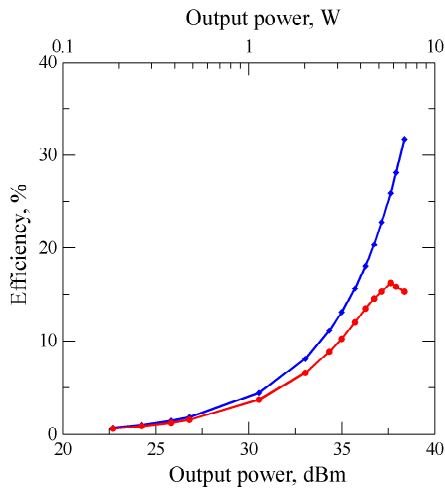


**Figure 7.** Drain and power-added efficiencies. The power-added efficiency at 5 W output is 15%.

ure 8. The total grid output and input powers are divided by the number of transistors in the grid, and the result is plotted against load-pull measurements of an isolated transistor to give an estimate of the grid combination efficiency. The combining loss at all power levels is close to 2 dB. We think it is likely that most of the combining loss results from the feedback resistor, and that it should be possible to reduce this loss.

### Concluding Remarks

A monolithic grid amplifier has been demonstrated with 8 dB small-signal gain, and 5 W of power at 5 dB gain at 37.2 GHz. Utilization of an aluminum-nitride heat spreader efficiently removes waste heat from the grid amplifier, allowing continuous operation with junction temperatures near 70°C, well below the maximum

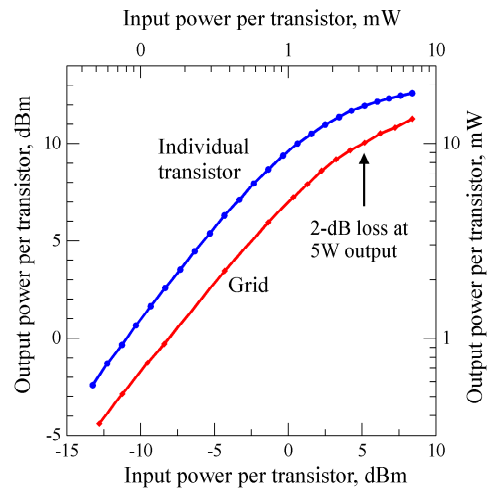


**Figure 8.** Combining loss. Grid input and output powers are normalized to the number of devices on the grid. Load-pull measurements for the isolated transistor were made at 39 GHz; the grid operates at 37.2 GHz.

temperature of 150°C. This indicates that it should be possible to make even more powerful grids.

### Acknowledgments

The authors appreciate the support from the Army Research Office through the Caltech Quasi-Optic Power Combining MURI, and DARPA MAFET program.

### References

- [1] C. M. Liu, E. A. Sovero, W. J. Ho, J. A. Higgins, M. P. Lisio, D. B. Rutledge, "Monolithic 40-GHz 670-mW HBT Grid Amplifier," *IEEE MTT-S Int. Microwave Symp. Dig.*, 1996, pp. 1123–1126.
- [2] E. A. Sovero, J. B. Hacker, J. A. Higgins, D. S. Deakin, A. L. Sailer, "A Ka-band Monolithic Quasi-Optic Amplifier," *IEEE MTT-S Int. Symp. Dig.*, 1998, pp. 1453–1456.
- [3] N. Cheng, T. Dao, M. G. Case, D. B. Rensch, R. A. York, "A 60-Watt Spatially Combined Solid-State Amplifier," *IEEE MTT-S Int. Symp. Dig.*, 1999, pp. 539–542.
- [4] J. Hubert, L. Mirth, S. Ortiz, A. Mortazawi, "A 4-Watt Ka-band Quasi-Optical Amplifier," *IEEE MTT-S Int. Symp. Dig.*, 1999, pp. 551–554.
- [5] P. Preventza, B. C. Dickman, E. A. Sovero, M. P. De Lisio, J. J. Rosenberg, D. B. Rutledge, "Modeling of Quasi-Optical Arrays," *IEEE Int. Symp., Dig.*, 1999, pp. 563–566.
- [6] C. M. Liu, M. P. De Lisio, A. Moussessian, D. B. Rutledge, "Stability of Grid Amplifiers," *IEEE Transactions on Microwave Theory and Techniques*, vol. 46, June 1998, pp. 769–774.